ChemComm

COMMUNICATION

View Article Online
View Journal | View Issue

Cite this: *Chem. Commun.*, 2016, 52, 1401

Received 15th November 2015,
Accepted 18th November 2015

DOI: 10.1039/c5cc09459c

www.rsc.org/chemcomm

A homochiral vanadium–salen based cadmium bpdc MOF with permanent porosity as an asymmetric catalyst in solvent-free cyanosilylation†

Asamanjoy Bhunia,[a] Subarna Dey,[b] José María Moreno,[c] Urbano Diaz,[c] Patricia Concepcion,[c] Kristof Van Hecke,[d] Christoph Janiak[b] and Pascal Van Der Voort*[a]

A homochiral vanadium–salen based MOF with the pcu topology is constructed *via in situ* synthesis under solvothermal conditions. The synthesized MOF exhibits BET surface areas of 574 $m^2 g^{-1}$, showing the highest H_2 adsorption capacity (1.05 wt% at 77 K, 1 bar) and the highest CO_2 uptake (51 $cm^3 g^{-1}$ at 273 K, 1 bar) for currently known salen-based MOFs. This framework shows excellent performance as an asymmetric catalyst in solvent-free cyanosilylation.

Metal organic frameworks (MOFs) are exciting hybrid materials for a plethora of potential applications including gas storage, gas separation, catalysis, and drug delivery.[1–3] They are crystalline nanoporous materials comprised of ordered networks formed from organic electron donor linkers and metal cations or clusters.[3] In MOF-based catalysis, either unsaturated metal coordination sites[4] or active linker sites in between the metals can be used as the catalytic active sites.[5,6] This second approach is much more challenging but offers unique opportunities to design highly selective and/or chiral catalysts. The most active linkers that have been developed to synthesize the chiral MOFs to date for asymmetric catalysis are based on BINOL and salen ligands.[6–9]

One possible strategy in the synthesis of chiral MOFs is the use of metalloligands.[7,10–12] In the metalloligand approach, metal-containing homo- and heteronuclear complexes (mostly salen types) that exhibit free coordination sites to connect to other metal atoms are allowed to form 1D, 2D or 3D networks. The additional linkers such as dicarboxylic or bipyridine groups are mostly used to construct a 3D structure that is mostly responsible for porosity.[10,11] Since metalloligands are more extended and flexible with respect to traditional organic linkers, it is however very hard to stabilize the framework. Although a few MOFs with salen struts have been examined as heterogeneous catalysis or as gas storage/separation vehicles, in most of the cases the framework suffered from severe diffusion limitations, even during the surface area measurements using nitrogen sorption.

Chen *et al.* reported several salen-containing MOFs called M'MOFs (mixed-metal organic frameworks) with surface areas ranging from 90 to 602 $m^2 g^{-1}$, albeit only measurable by the CO_2 uptake at 195 K.[10,11] The authors argued that the N_2 adsorption at 77 K on the activated M'MOFs was too slow because of diffusion effects. On the other hand, Hupp *et al.* reported that the surface area of the Mn^{III}SO-MOFs and Mn^{II}SO-MOFs was 478 and 385 $m^2 g^{-1}$ using N_2 adsorption at 77 K.[13]

Many examples of asymmetric catalysis have been used by chiral MOFs for the synthesis of chiral molecules while metal centers in the metallosalen linkers are catalytically active. Cui *et al.* reported hydrolytic kinetic resolution and chiral sulfoxidation reactions for Co– and Ti–salen based MOFs, respectively, but again the N_2 sorption of their frameworks at 77 K showed only surface adsorption.[14,15] Hupp and Lin reported Mn– and Ru–salen MOFs for asymmetric catalytic alkene epoxidation and cyclopropanation reactions.[5,12,16] However, these MOFs also did not show permanent porosity. Therefore, the synthesis of permanently porous salen-based chiral frameworks is a huge challenge for asymmetric catalysis and gas sorption within the same frameworks.

In the last few years, one of the most important and rapidly growing concepts has been the development of green synthesis methods that are efficient, selective, high yielding and environmentally favorable.[17,18] Therefore, solvent-free reaction conditions offer significant advantages such as decreased energy consumption, reduced reaction times, fewer by-products, no purification and a large reduction in the reactor size. Also, one-step *in situ*

[a] *Department of Inorganic and Physical Chemistry, Center for Ordered Materials, Organometallics and Catalysis, Ghent University, Krijgslaan 281-S3, 9000 Ghent, Belgium. E-mail: pascal.vandervoort@ugent.be*
[b] *Institut für Anorganische Chemie und Strukturchemie, Universität Düsseldorf, 40204 Düsseldorf, Germany*
[c] *Instituto de Tecnología Quimica (UPV-CSIC), Avenida de los Naranjos s/n, 46022 Valencia, Spain*
[d] *Department of Inorganic and Physical Chemistry, Ghent University, Krijgslaan 281-S3, 9000 Ghent, Belgium*

† Electronic supplementary information (ESI) available: Experimental details, characterization data, solvent-free cyanosilylation, crystallographic data (CIF), and additional tables and figures. CCDC 1422004. For ESI and crystallographic data in CIF or other electronic format see DOI: 10.1039/c5cc09459c

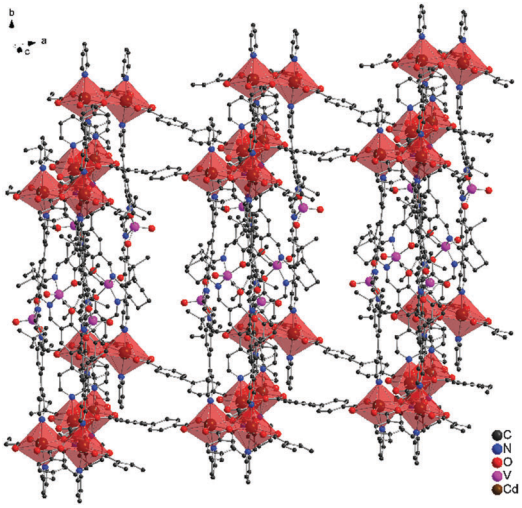

Fig. 1 Section of the packing of V–salen Cd-bpdc MOF from a single-crystal X-ray structure (hydrogen atoms omitted for clarity). Polyhedra depict the edge-sharing pentagonal bipyramidal coordination environment around two adjacent Cd atoms.

processes save time and consumables. Therefore, *in situ* synthesis as well as solvent-free organic transformation is a great challenge in current research.

Herein, we report a chiral vanadium–salen based Cd-MOF using the chiral ligand (*R*,*R*)-(−)-1,2-cyclohexanediamino-*N*,*N*′-bis(3-*tert*-butyl-5-(4-pyridyl)salicylidene) (H_2L) *via in situ* synthesis under solvothermal conditions instead of a multi-step[19] process. We tested its potential application in solvent-free cyanosilylation catalysis and its gas adsorption properties.

The reaction of the chiral ligand H_2L, $VOSO_4$, $Cd(NO_3)_2{\cdot}(H_2O)_4$ and biphenyl-4,4′-dicarboxylic acid (bpdc) in the presence of DMF/EtOH/H_2O at 100 °C resulted in the formation of a 3D MOF (see the ESI† for synthesis and characterization). This compound was characterized by standard analytical/spectroscopic techniques and the solid-state structure was determined by single-crystal X-ray diffraction techniques (Fig. 1).‡ The resulting product is stable in air and insoluble in common organic solvents such as chloroform, acetone, acetonitrile, THF, MeOH, EtOH, *etc.* The bulk purity of the compound was confirmed by a comparison of their activated and X-ray diffraction simulated powder (PXRD) patterns (Fig. S2 in the ESI†). From thermogravimetric (TG) analysis, it was observed that the activated compound starts to decompose with significant weight loss only above 350 °C (Fig. S3 in the ESI†).

Single-crystal X-ray crystallography showed that the compound crystallized in the orthorhombic non-centrosymmetric space group $P222_1$.[19] The asymmetric unit consists of two cadmium(II) ions, two V–salen units ($V^{IV}OL$), and two biphenyldicarboxylate ligands (bpdc). However, both the linkers (VO–salen and bpdc) are parallel to each other in the 1D channel of the framework in which a distorted rectangular aperture of $\sim 7 \times 3.5$ Å^2 along the *a* direction (considering the van der Waals radii of the H and C wall atoms) is estimated, respectively (Fig. S18, ESI†). The guest solvent molecules in the channel could not be determined by X-ray crystallography due to their disordered nature, so that the Squeeze option in PLATON was utilized (see the details in the ESI†). Each cadmium(II) atom is hepta-coordinated by five oxygen atoms from three carboxylate groups of bpdc ligands and two nitrogen atoms from the V–salen pyridine units. Two neighboring cadmium(II) atoms are bridged by two μ_2-η^2:η^1 bpdc carboxylate groups and form a secondary building block (SBU) leading to the formation of a 3D network with a **pcu** topology (Fig. S16 and S17, ESI†). In the V–salen unit, oxygen atoms and the vanadium(IV) atom are disordered over two positions.[20,21] As expected, in the center of each salen ligand, the vanadium(IV) atom adopts a distorted square pyramidal coordination geometry. The framework topology was simplified to its underlying net, using the ToposPro program package (see the framework topology in the ESI† for full details).[22] The structure shows two equivalent, interpenetrating frameworks (Fig. S11, ESI†). In the standard representation, the underlying net of each framework (Fig. S12, ESI†) can be considered to be a 2-nodal 3,5-coordinated net with (3-c)(5-c) nodes stoichiometry, resulting in the formation of a **fet** topology (Fig. S13, ESI†), while in the cluster representation, a uninodal 6-coordinated net with the **pcu** topology (Fig. S16, ESI†) is observed, with 4 short edges (16.8 Å) and two long, double bridged, opposite (*trans*) edges (24.0 Å) (running down the [010] direction).

The porosity was characterized by standard N_2 sorption measurements at 77 K. The material was activated by degassing at 100 °C under high vacuum (10^{-6} Torr) for 24 h. The isotherm shows a steep slope at low P/P_0 values with a type I isotherm, which is typical for microporous materials (Fig. 2).[23,24]

The calculated Langmuir and BET surface area were found to be 697 and 574 m^2 g^{-1}, respectively. The total pore volume was estimated to be 0.24 cm^3 g^{-1} at a relative pressure $P/P_0 = 0.97$. The absence of hysteresis during the adsorption and desorption points indicated that the framework was stable as well as rigid. To the best of our knowledge, this compound exhibits the highest surface area amongst all metalloligand-based MOFs characterized by standard nitrogen sorption (*i.e.* at 77 K) (Table S1, ESI†). Even, the surface area lies in the upper end when compared to other M'MOFs that showed BET surface areas (measured by CO_2

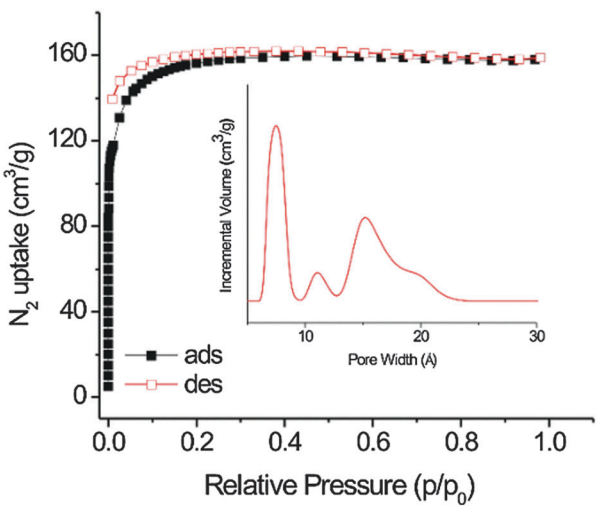

Fig. 2 N_2 sorption isotherm at 77 K. Inset: NL-DFT pore-size distribution curve of V–salen Cd-bpdc MOF.

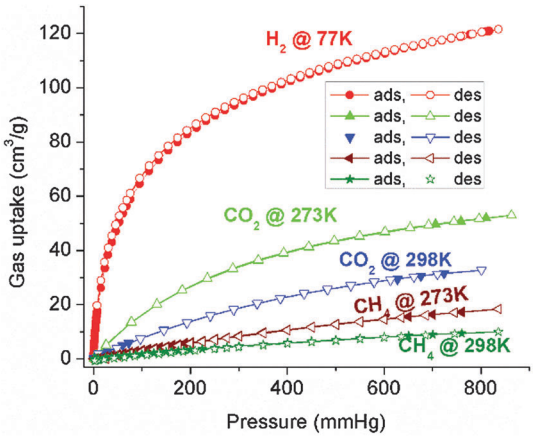

Fig. 3 Low-pressure H_2, CO_2 and CH_4 sorption isotherms.

Table 1 Asymmetric cyanosilylation of aldehydes catalyzed by vanadium–salen Cd-bpdc MOF[a]

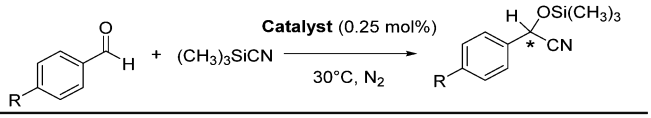

Entry	R	Time	Yield[b] (%)	ee[c] (%)
1	H	14	95	78
2	Me	14	93	76
3	OMe	14	76	80
4	Cl	14	98	72
5	Br	14	98	76
6[d]	H	9	91	57

[a] Reaction conditions: catalyst (0.25 mol%), aldehyde (0.82 mmol) and trimethylsilyl cyanide (3 eq.), and time 14 h. [b] Calculated by GC. [c] Determined by chiral GC. [d] Catalyst: VO–salen in the homogeneous phase.

at 195 K) of 90–602 $m^2\ g^{-1}$.[10,11] The pore size distribution was determined by non-local density functional theory (NL-DFT) using a slit-pore model based on the N_2 adsorption isotherms. A narrow distribution of micropores centered at 7, 11, and 15 Å were observed (inset in Fig. 2). However, the major peak was at 7 Å, which matches with the calculated value (Fig. S19, ESI†) obtained from the single-crystal structure (ultramicropores <7 Å cannot be detected from N_2 sorption isotherms).

Because of the porosity of the V–salen Cd-bpdc MOF, as well as the large number of nitrogen atoms (imine and pyridine nitrogen atoms) in the framework, we decided to examine its adsorption properties at low pressure (*i.e.* 1 bar) for CO_2 and other gases (*i.e.* H_2 and CH_4). The CO_2 adsorption capacities in the activated material are 51 $cm^3\ g^{-1}$ at 273 K and 32 $cm^3\ g^{-1}$ at 298 K (Fig. 3), which is again higher than that of any known M'MOF material.[10,11]

To further understand the adsorption properties, the isosteric heats of adsorption were calculated from the CO_2 adsorption isotherms at 273 K and 298 K (Fig. S4, ESI†), as they describe the interaction with the hydrophobic pore surfaces. At zero loading the Q_{st} value ($-\Delta H$) is 30 kJ mol^{-1}. Upon increasing the loading the Q_{st} value decreases rapidly to 28 kJ mol^{-1}, which is still well above the heat of liquefaction of bulk CO_2 with 17 kJ mol^{-1} or the isosteric enthalpy of adsorption for CO_2 on activated carbons (*e.g.* BPL 25.7 kJ mol^{-1}, A10 21.6 kJ mol^{-1}, Norit R1 Extra 22.0 kJ mol^{-1}).[25,26] The high Q_{st} value can be attributed to the high polar framework and the pore size effect. The high adsorption enthalpy at zero coverage is explained by the initial filling of the small ultramicropores with 4 Å diameter (Fig. S5, ESI†) with adsorbate–surface interactions on both sides or ends of the CO_2 molecules. In contrast to CO_2, only 17 and 9 $cm^3\ g^{-1}$ of nonpolar CH_4 were adsorbed at 273 and 298 K. Interestingly, the material adsorbs 120 $cm^3\ g^{-1}$ (or 1.05 wt%) H_2 at 77 K and 1 bar (Fig. 3). This uptake is higher than that of other M'MOF materials, and it is mainly due to size exclusion effects.

We wished to examine if the VO–salen unit was accessible for asymmetric catalytic reactions (Table 1). Therefore, we studied the catalytic activity for cyanosilylation reactions of aromatic aldehydes under solvent-free conditions. However, chiral VO-salen complexes are active homogeneous asymmetric catalysts for various types of organic reactions.[27] To optimize the reaction conditions, the study was carried out in the reaction of benzaldehyde (0.82 mmol) and trimethylsilyl cyanide (2.46 mmol) by using 0.25 mol% catalyst in an N_2 atmosphere at 30 °C. The resulting yield of the reaction reached up to 95% after 14 h. Upon increasing the time, the yield of the reaction did not improve, the cyanosilylation reaction being performed with a 1:3 mol ratio of the selected aldehyde and TMSCN in an N_2 atmosphere at 30 °C for 14 h as the optimal working conditions (Fig. S6 and ESI†). To confirm the leaching, the catalyst is separated by filtration or centrifugation when the yield reaches 35% and then the reaction was continued (hot filtration test) (Fig. S6 in the ESI†). After 14 h, we observed that the reaction yield did not increase further.

MOF materials are structured from coordination bonds between metallic clusters and organic ligands that can be easily modified upon contact with organic solvents. In fact, leaching phenomena are frequently observed when solid MOF catalysts are used in different catalytic processes. In our case, the use of solvent-free conditions, during the cyanosilylation of aldehydes, favors the preservation of the V–salen-MOF structure, avoiding the decomposition and disorganization of the pristine MOF, and preventing the presence of homogeneous active sites in the reaction media. Experiments carried out in the presence of different solvents (chloroform and acetonitrile) confirmed this fact because leaching is clearly detected, showing the convenience of avoiding the use of organic solvents during the catalytic processes (Fig. S10a and b in ESI†). Further, chiral centers are influenced by their chemical environment. The presence of organic solvents as the reaction medium together with the hydrophobic properties of MOF materials could favor the excessive presence of solvent molecules adsorbed around chiral active sites. The consequence could be an activity decrease of asymmetric centers. Considering this, solvent-free conditions would be preferred for chiral solid catalysts. Therefore, we investigated the catalytic reaction in the absence of any solvent. Under these optimized conditions, the cyanosilylation of benzaldehyde gave 95% yield with 78% ee (Fig. 4 and Table 1), which is high compared with the recent work by the Duan and Cui groups.[19,28] They carried out the heterogeneous asymmetric cyanosilylation reaction by using an organic solvent such as CH_3CN and DCM.

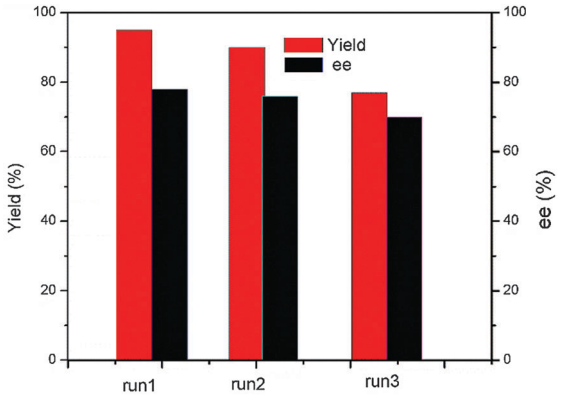

Fig. 4 Yield and enantiomeric excess (ee) for cyanosilylation reaction of benzaldehyde during 1st, 2nd and 3rd runs.

Even, the Cui group used Ph_3PO as a base to promote cyanosilylation.[19] To the best of our knowledge, no solvent-free cyanosilylation has been reported for salen-based MOFs. In our study, we not only use solvent-free conditions, but also a smaller amount of the catalyst. Moreover, the heterogeneous nature of the reaction was further confirmed by recyclability and reusability tests of the catalyst in the cyanosilylation of benzaldehyde (Fig. 4 and Fig. S6, S7 in the ESI†). We observed that the activity was maintained for the following two runs without significant change in the ee value (Fig. 4 and Table S2, ESI†). In the 3rd run, the yield and ee were decreased, which is associated with the modification of the surrounding environment of chiral centers or undesirable adsorption of organic compounds. After the 3rd run, the catalyst still maintained its crystalline structure, which was confirmed by PXRD (Fig. S7, ESI†). Moreover, the UV-vis spectrum of the fresh and reused catalyst (after the 3rd run) did not show remarkable changes in the vanadium species (Fig. S7, ESI†). In order to prove the effect of introduction of different substituents in the aromatic ring at the *para*-position, we further used aromatic aldehydes with an electron-withdrawing (–Cl and –Br) and an electron-donating (–Me and –OMe) group (Table 1 and Fig. S8 in the ESI†). The electron-withdrawing (–Cl and –Br) group gave higher yield whereas the electron-donating group decreased the yield with respect to benzaldehyde. This tendency is explained by the higher electropositive charge on the carbonyl group of aldehyde achieved in the presence of electron-withdrawing groups, resulting in a higher activation of the substrate. In contrast, for the electron-donating group, the activation of the carbonyl group is lower. Moreover, in all cases the ee value is higher than 72% (Table 1).

In conclusion, we have reported a chiral vanadium–salen based Cd-bpdc MOF using a chiral salen ligand (*R*,*R*)-(−)-1,2-cyclohexanediamino-*N*,*N*′-bis(3-*tert*-butyl-5-(4-pyridyl)salicylidene) (H_2L) *via in situ* synthesis under solvothermal conditions. This MOF shows to be intrinsically microporous with a high BET surface area of 574 $m^2\ g^{-1}$. At 273 K and 1 bar, this framework exhibits a higher CO_2 uptake capacity than other metallosalen-based MOFs. We tested this compound as a chiral catalyst for asymmetric cyanosilylation of aromatic aldehydes under solvent-free conditions. The catalyst is recyclable and reusable and showed a good conversion and ee. This green and solvent-free approach can be highly suitable for the synthesis of various chiral products such as α-hydroxy acids, α-hydroxy aldehydes and β-amino alcohols through the corresponding cyanohydrin in biomedicinal chemistry.

This research was funded by Ghent University, GOA grant number 01G00710.

Notes and references

‡ Crystal data for V–salen Cd-bpdc MOF: $C_{104}H_{100}Cd_2N_8O_{13\cdot63}V_2$, M = 2006.69, orthorhombic, space group $P2221$ (No. 17), a = 17.0460(5) Å, b = 24.0462(6) Å, c = 28.8442(6) Å, V = 11823.0(5) $Å^3$, Z = 4, T = 100 K, ρ_{calc} = 1.127 g cm^{-3}, μ(Cu-Kα) = 4.565 mm^{-1}, $F(000)$ = 4124.1, 68 492 reflections measured, 24 063 unique (R_{int} = 0.0926), which were used in all calculations. The final R_1 was 0.0564 ($I > 2\sigma(I)$) and wR_2 was 0.1393 (all data). CCDC 1422004.

1 H. Furukawa, K. E. Cordova, M. O'Keeffe and O. M. Yaghi, *Science*, 2013, **341**, 1230444.
2 K. Sumida, D. L. Rogow, J. A. Mason, T. M. McDonald, E. D. Bloch, Z. R. Herm, T.-H. Bae and J. R. Long, *Chem. Rev.*, 2012, **112**, 724–781.
3 G. Férey, *Chem. Soc. Rev.*, 2008, **37**, 191–214.
4 A. Corma, H. García and F. X. Llabrés i Xamena, *Chem. Rev.*, 2010, **110**, 4606–4655.
5 S.-H. Cho, B. Ma, S. T. Nguyen, J. T. Hupp and T. E. Albrecht-Schmitt, *Chem. Commun.*, 2006, 2563–2565.
6 L. Ma, J. M. Falkowski, C. Abney and W. Lin, *Nat. Chem.*, 2010, **2**, 838–846.
7 R. Kitaura, G. Onoyama, H. Sakamoto, R. Matsuda, S.-I. Noro and S. Kitagawa, *Angew. Chem., Int. Ed.*, 2004, **43**, 2684–2687.
8 A. Bhunia, Y. Lan, V. Mereacre, M. T. Gamer, A. K. Powell and P. W. Roesky, *Inorg. Chem.*, 2011, **50**, 12697–12704.
9 A. Bhunia, M. A. Gotthardt, M. Yadav, M. T. Gamer, A. Eichhöfer, W. Kleist and P. W. Roesky, *Chem. – Eur. J.*, 2013, **19**, 1986–1995.
10 S.-C. Xiang, Z. Zhang, C.-G. Zhao, K. Hong, X. Zhao, D.-R. Ding, M.-H. Xie, C.-D. Wu, M. C. Das, R. Gill, K. M. Thomas and B. Chen, *Nat. Commun.*, 2011, **2**, 204.
11 M. C. Das, Q. Guo, Y. He, J. Kim, C.-G. Zhao, K. Hong, S. Xiang, Z. Zhang, K. M. Thomas, R. Krishna and B. Chen, *J. Am. Chem. Soc.*, 2012, **134**, 8703–8710.
12 F. Song, C. Wang, J. M. Falkowski, L. Ma and W. Lin, *J. Am. Chem. Soc.*, 2010, **132**, 15390–15398.
13 A. M. Shultz, A. A. Sarjeant, O. K. Farha, J. T. Hupp and S. T. Nguyen, *J. Am. Chem. Soc.*, 2011, **133**, 13252–13255.
14 C. Zhu, G. Yuan, X. Chen, Z. Yang and Y. Cui, *J. Am. Chem. Soc.*, 2012, **134**, 8058–8061.
15 W. Xuan, C. Ye, M. Zhang, Z. Chen and Y. Cui, *Chem. Sci.*, 2013, **4**, 3154–3159.
16 J. M. Falkowski, C. Wang, S. Liu and W. Lin, *Angew. Chem., Int. Ed.*, 2011, **50**, 8674–8678.
17 J. M. DeSimone, *Science*, 2002, **297**, 799–803.
18 P. J. Walsh, H. Li and C. A. de Parrodi, *Chem. Rev.*, 2007, **107**, 2503–2545.
19 W. Xi, Y. Liu, Q. Xia, Z. Li and Y. Cui, *Chem. – Eur. J.*, 2015, **21**, 12581–12585.
20 Y. N. Belokon, P. Carta, A. V. Gutnov, V. Maleev, M. A. Moskalenko, L. V. Yashkina, N. S. Ikonnikov, N. V. Voskoboev, V. N. Khrustalev and M. North, *Helv. Chim. Acta*, 2002, **85**, 3301–3312.
21 P. Adão, J. Costa Pessoa, R. T. Henriques, M. L. Kuznetsov, F. Avecilla, M. R. Maurya, U. Kumar and I. Correia, *Inorg. Chem.*, 2009, **48**, 3542–3561.
22 V. A. Blatov, A. P. Shevchenko and D. M. Proserpio, *Cryst. Growth Des.*, 2014, **14**, 3576–3586.
23 K. S. W. Sing, D. H. Everett, R. A. W. Haul, L. Moscou, R. A. Pierotti, J. Rouquerol and T. Siemieniewska, *Pure Appl. Chem.*, 1985, **57**, 603–619.
24 G. Leofanti, M. Padovan, G. Tozzola and B. Venturelli, *Catal. Today*, 1998, **41**, 207–219.
25 K. B. Lee, M. G. Beaver, H. S. Caram and S. Sircar, *Ind. Eng. Chem. Res.*, 2008, **47**, 8048–8062.
26 S. Himeno, T. Komatsu and S. Fujita, *J. Chem. Eng. Data*, 2005, **50**, 369–376.
27 (*a*) V. Chechik, M. Conte, T. Dransfield, M. North and M. Omedes-Pujol, *Chem. Commun.*, 2010, **46**, 3372–3374; (*b*) Y. N. Belokon, M. North and T. Parsons, *Org. Lett.*, 2000, **2**, 1617–1619.
28 D. Dang, P. Wu, C. He, Z. Xie and C. Duan, *J. Am. Chem. Soc.*, 2010, **132**, 14321–14323.

